Journal Pre-proof

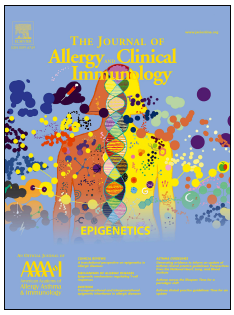

Janus kinase inhibition for autoinflammation in DNASE2 deficiency

Ying Hong, PhD, Melania Capitani, PhD, Claire Murphy, PhD, Sumeet Pandey, PhD, Athena Cavounidis, MSc, Haruo Takeshita, PhD, Sira Nanthapisal, PhD, Toshihiro Yasuda, PhD, Brigitte Bader-Meunier, MD, Dara McCreary, MSc, Ebun Omoyinmi, PhD, Anupama Rao, MD, Claire Booth, PhD, Kimberly Gilmour, PhD, Neil Sebire, PhD, Neil Shah, PhD, Nigel Klein, PhD, Alex N. Bullock, PhD, Despina Eleftheriou, PhD, Holm H. Uhlig, MD, DPhil, Paul Brogan, PhD

PII: S0091-6749(19)31602-1

DOI: https://doi.org/10.1016/j.jaci.2019.11.020

Reference: YMAI 14275

To appear in: *Journal of Allergy and Clinical Immunology*

Received Date: 22 August 2019

Revised Date: 13 November 2019

Accepted Date: 15 November 2019

Please cite this article as: Hong Y, Capitani M, Murphy C, Pandey S, Cavounidis A, Takeshita H, Nanthapisal S, Yasuda T, Bader-Meunier B, McCreary D, Omoyinmi E, Rao A, Booth C, Gilmour K, Sebire N, Shah N, Klein N, Bullock AN, Eleftheriou D, Uhlig HH, Brogan P, Janus kinase inhibition for autoinflammation in DNASE2 deficiency, *Journal of Allergy and Clinical Immunology* (2019), doi: https://doi.org/10.1016/j.jaci.2019.11.020.

Title: Janus kinase inhibition for autoinflammation in DNASE2 deficiency

Authors: [1]Ying Hong PhD[*], [2]Melania Capitani PhD [*], [1,3]Claire Murphy PhD, [2]Sumeet Pandey PhD , [2]Athena Cavounidis MSc, [4]Haruo Takeshita PhD, [1,5]Sira Nanthapisal PhD, [6]Toshihiro Yasuda PhD, [7]Brigitte Bader-Meunier MD, [1]Dara McCreary MSc, [1]Ebun Omoyinmi PhD, [3]Anupama Rao MD, [1,3]Claire Booth PhD, [3]Kimberly Gilmour PhD, [3]Neil Sebire PhD, [3]Neil Shah PhD, [1,3]Nigel Klein PhD, [8]Alex N Bullock PhD, [1,3,9] Despina Eleftheriou PhD, [2]Holm H Uhlig MD, DPhil [**]and [1,3]Paul Brogan PhD [**].

Affiliations: [1] University College London Great Ormond Street Institute of Child Health, London, United Kingdom; [2] Translational Gastroenterology Unit, University of Oxford, Oxford, United Kingdom and Department of Pediatrics, University of Oxford, Oxford, United Kingdom and Oxford Biomedical Research Centre (BRC), University of Oxford; [3] Great Ormond Street Hospital for Children NHS Foundation Trust, London, United Kingdom; [4] Department of Legal Medicine, Shimane University, Japan; [5] Thammasat University, Thailand; [6] Department of Medical Genetics and Biochemistry, University of Fukui, Japan; [7] Department of Pediatic Immunology and Rheumatology, Hôpital Necker-Enfants Malades, Assistance Publique-Hôpitaux de Paris, Paris, 75015, France ; [8] Structural Genomics Consortium, Nuffield Department of Medicine, University of Oxford, Oxford, United Kingdom; [9] Arthritis Research UK centre for adolescent rheumatology, UCL, London, United Kingdom.

*** and ** equal contribution**

Corresponding Author: Ying Hong, UCL GOS Institute of Child Health, 30 Guilford Street, London WC1N 1EH, UK. Email: y.hong@ucl.ac.uk. Tel: 00442079052392.

Disclosures: PB has received institutional grants from: Novartis, SOBI, Roche, Chemocentryx, and Novimmune; consultancy fees from Roche, Novartis and SOBI; and speaker fees from UCB. DE received institutional grants from Lilly, Roche and Pfizer. HHU received research support or consultancy fees from UCB Pharma, Eli Lilly, Boehringer Ingelheim, Pfizer, Celgene, and AbbVie. CB received consultancy fees from Novimmune and SOBI. All research at Great Ormond Street Hospital NHS Foundation Trust and UCL Great Ormond Street Institute of Child Health is made possible by the NIHR Great Ormond Street Hospital Biomedical Research Centre. The views expressed are those of the author(s) and not necessarily those of the NHS, the NIHR or the Department of Health.

Acknowledgements: This work was funded in part by Rosetrees, Great Ormond Street Hospital Children's Charity and Versus Arthritis (grant 21791, 21593 and 21064). All research at Great Ormond Street Hospital NHS Foundation Trust and UCL Great Ormond Street Institute of Child Health is made possible by the NIHR Great Ormond Street Hospital Biomedical Research Centre. We acknowledge support for set-up of pilot experiments by the BRC to the Oxford GI biobank (11/YH/0020, 16/YH/0247). The research was also supported by the National Institute for Health Research (NIHR) Oxford Biomedical Research Centre (BRC), University of Oxford and the Structural Genomics Consortium SGC. HHU is supported the Health Research (NIHR) Oxford Biomedical Research Centre and the The Leona M. and Harry B. Helmsley Charitable Trust. We would like to thank the patients and their families as well as healthy volunteers for consenting to this research. We would like to thank Yanick Crow, Jan Rehwinkel, Anne Bridgeman, Jonny Hertzog and Julie Schulthess for the critical inputs and research materials.

Capsule summary: We characterise the immunopathogenesis of autoinflammation, HLH, and early onset intestinal inflammation caused by homozygous mutation in *DNASE2*, and provide the first description of favourable therapeutic response to JAK1/JAK2 blockade in this disease.

Key Words: DNASE2 deficiency; Type I Interferon; autoinflammation; JAK inhibition; baricitinib; haemophagocytic lymphohistiocytosis; early-onset intestinal inflammation.

To the Editor,

Defective elimination of nucleic acids can trigger autoinflammatory and autoimmune processes (1). Mice lacking the lysosomal endonucleases DNase-II have shown intracellular DNA accumulation leading to severe anemia and embryonic death (2). Humans carrying homozygous non-synonymous loss-of-function mutations in *DNASE2* complete gestation, but are severely affected by congenital anemia and an inflammatory disorder characterised by splenomegaly, glomerulonephritis, liver fibrosis, circulating anti-DNA auto-antibodies, and progressive arthritis (3).

We describe a patient with a novel hypomorphic homozygous missense mutation in *DNASE2* (c.A284G; p.Y95C) resulting in severe autoinflammation, failure to thrive, haemophagocytic lymphohistiocytosis (HLH), early-onset chronic intestinal inflammation, and suppression of haematopoiesis. Beyond the recent description of this disorder on 3 patients (3), we further characterize cytokine dysregulation and demonstrate successful treatment with the Janus kinase 1/2 inhibitor baricitinib.

The proband (V-2) is a 14-year-old Somalian girl from endogamous kindred with a history of neonatal anemia (**Fig. 1A**). At 6 years of age, patient V-2 was referred for pyrexia; a history of pancytopenia, hepatosplenomegaly, failure to thrive (height and weight below the 0.4^{th} percentile), chronic diarrhoea and delayed motor skill development. Investigations (summarized in **Table S1**) revealed severe pancytopenia, requiring multiple transfusions of red cells and platelets. Intestinal histology from endoscopic biopsies revealed multiple granuloma-like cells within mucosa-associated lymphoid tissue, compatible with phagocytosed DNA fragments (pseudo-granuloma). Magnetic resonance imaging of the brain revealed bi-parietal deep white matter parenchymal signal abnormalities (**Fig. 1B**). Bone marrow studies identified macrophage infiltration and associated haemophagocytosis (**Fig. 1C**). At 9 years of age, the patient experienced severe Epstein Barr virus infection, necessitating treatment with dexamethasone and rituximab. Typical HLH criteria were met (**Table S1)**. She responded partially to the HLH-2004 chemotherapy treatment protocol which she had for 7 weeks (4) with cessation of fever, and improvement in diarrhoea, but with ongoing pancytopenia and hepato-splenomegaly. For several years, transfusion-dependent anemia, chronic diarrhoea, and severe growth retardation were observed.

Homozygosity mapping and whole exome sequencing revealed a rare homozygous variant in *DNASE2* (c.284A>G; p.Y95C; **Table S2, Fig. S1A**). The affected variant is highly conserved

across species (**Fig. 1D**). We used structural data of existing DNase-II homodimer complexed with double-stranded DNA crystal structure from *Burkholderia thailandensis* to model the human DNase-II (5). Residue Y95 is closely packed with residue T114, which is central to the nuclease catalytic HxK motif (H113 and K115) suggesting that small perturbations at residue 95 may have significant impact on catalytic activity. The two recently published mutations in *DNASE2* (p.G116A and p.D121V) (3) will likely disrupt the same catalytic domain (**Fig. 1E**).

The p.Y95C variant completely abolishes DNase-II activity in a single radial enzyme diffusion (**Fig. S1B**) and confers loss-of-function of the protein rather than absence (**Fig. S1C-D**). Furthermore, granulocyte lysates from V-2 confirmed a deficiency in degrading DNA (**Fig. 1F)**.

Macrophages show highest expression of *DNASE2* and are most likely affected in DNase-II deficient patients (**Fig. S2A).** We observed increased lysosomal DNA accumulation in monocyte-derived macrophages from V-2 compared to controls, (**Fig. S2B**). Similarly, clearance of exogenous apoptotic or bacterial derived DNA was reduced in V-2 macrophages (**Fig. S2C-2D**). To investigate whether DNase-II deficiency causes a selective DNA degradation defect or broadly affects lysosomal function, we tested antimicrobial activity in V-2 macrophages (**Fig. S2E**). Normal antimicrobial activity suggests that the defect in *DNASE2* patients is restricted to the inability to clear DNA.

Previous studies emphasized that deficiency in *DNASE2* in humans and mice results in the induction of interferon, and non-interferon-mediated inflammation (2,3,6,7). Elevated levels of TNF, MCP-1, IL-18, IFN-2α, IFN-β, and IFN-γ were detected in sera of V-2 (**Fig. 1G**). Increased levels of TNF, IL-1β, IP-10 and IL-8 were observed in V-2 fibroblasts (**Fig. S3A**). p.Y95C macrophages showed high levels of TNF and IL18, modestly increased IL-1β, and a clear induction of type I IFNs (**Fig. S3B**), which we also confirmed to be present in one of the previously described patients (3) (**Fig. S3B**).

Type I interferons (IFN-α and IFN-β) bind to type I receptors (IFNAR1/2) and induce the activation of JAK1 and TYK2, leading to STAT1 and STAT2 phosphorylation and interferon stimulated gene (ISG) expression (8). Since the immunotype of V-2 was indicative of a strong ISG signature, we explored JAK inhibition as a therapeutic option. *In vitro* JAK1/JAK2 blockade with baricitinib reduced ISG expression in fibroblasts from controls, patient V-2, and control macrophages following IFN-α stimulation (**Fig. S4A-B**). In contrast, selective blockade of JAK2 using AG490 did not revert the ISG signature **(Fig. S4A).** In healthy macrophages,

baricitinib treatment had stronger effects on ISG reduction compared to fibroblasts **(Fig. S4B)**. IFN-α-induced IL18 levels were reduced following baricitinib or AG490 treatment **(Fig. S4C),** suggesting a contribution of JAK2 signalling to IL18 production in control macrophages.

Since JAK inhibitors are effective in several interferonopathies (9), and baricitinib reverted the inflammatory signature in fibroblasts and macrophages *in vitro*, we treated our otherwise therapy non-responsive patient with baricitinib. We started with 2mg oral dose once daily, increasing weekly by 2 mg to achieve a final target dose of 2 mg, 3 times a day. Baricitinib was well tolerated with no adverse events, and resulted in a rapid and sustained clinical improvement (now for over 6 months). In particular, the improved energy levels reported by the patient and the ability to attend school full-time were relevant patient reported outcomes. Weight gain improved (**Fig. 2A**), and the patient underwent menarche 4 months after starting baricitinib. Blood parameters (**Fig. 2B**), gastrointestinal symptoms, and faecal calprotectin levels improved (**Fig. 2B**). Baricitinib decreased ISG expression in the peripheral blood and cytokine levels compared to pre-treatment levels (**Fig. 2C-E**). After 6 months of treatment, however, whilst the ISG signature indicated normalisation of SIGLEC1 and ISG15, there was an upward trend of IFIT1, IFI44L, RSDA2, IL-18 and IFI27 despite ongoing therapeutic response. Our data suggest that JAK1/2 inhibition is a rational and effective treatment for DNase-II deficiency.

In conclusion, we describe an additional patient with human DNase-II deficiency who presented with HLH and early-onset intestinal inflammation, expanding the phenotype spectrum of DNase-II deficiency. We characterize the mechanisms underpinning the complex immunophenotype, and show in a single patient that blocking JAK1/JAK2 with baricitinib can be used to curb pathological interferon signaling caused by an inability to clear intracellular DNA.

Ying Hong PhD

Melania Capitani PhD

Claire Murphy PhD

Sumeet Pandey PhD

Athena Cavounidis MSc

Haruo Takeshita PhD

Sira Nanthapisal PhD

Toshihiro Yasuda PhD

Brigitte Bader-Meunier MD

Dara McCreary MSc

Ebun Omoyinmi PhD

Anupama Rao MD

Claire Booth PhD

Kimberly Gilmour PhD

Neil Sebire PhD

Neil Shah PhD

Nigel Klein PhD

Alex N Bullock PhD

Despina Eleftheriou PhD

Holm H Uhlig MD, DPhil

Paul Brogan PhD

REFERENCES

1. Lazear HM, Schoggins JW, Diamond MS. Shared and Distinct Functions of Type I and Type III Interferons. Immunity. 2019 Apr;50(4):907–23.

2. Kawane K. Requirement of DNase II for Definitive Erythropoiesis in the Mouse Fetal Liver. Science. 2001 May 25;292(5521):1546–9.

3. Rodero MP, Tesser A, Bartok E, Rice GI, Della Mina E, Depp M, et al. Type I interferon-mediated autoinflammation due to DNase II deficiency. Nat Commun [Internet]. 2017 Dec [cited 2018 May 9];8(1). Available from: http://www.nature.com/articles/s41467-017-01932-3

4. Henter J-I, Horne A, Aricó M, Egeler RM, Filipovich AH, Imashuku S, et al. HLH-2004: Diagnostic and therapeutic guidelines for hemophagocytic lymphohistiocytosis. Pediatr Blood Cancer. 2007 Feb;48(2):124–31.

5. Varela-Ramirez A, Abendroth J, Mejia AA, Phan IQ, Lorimer DD, Edwards TE, et al. Structure of acid deoxyribonuclease. Nucleic Acids Res. 2017 Jun 2;45(10):6217–27.

6. Pawaria S, Moody K, Busto P, Nündel K, Choi C-H, Ghayur T, et al. Cutting Edge: DNase II Deficiency Prevents Activation of Autoreactive B Cells by Double-Stranded DNA Endogenous Ligands. J Immunol. 2015 Feb 15;194(4):1403–7.

7. Kawane K, Tanaka H, Kitahara Y, Shimaoka S, Nagata S. Cytokine-dependent but acquired immunity-independent arthritis caused by DNA escaped from degradation. Proc Natl Acad Sci. 2010 Nov 9;107(45):19432–7.

8. Ivashkiv LB, Donlin LT. Regulation of type I interferon responses. Nat Rev Immunol. 2014 Jan;14(1):36–49.

9. Sanchez GAM, Reinhardt A, Ramsey S, Wittkowski H, Hashkes PJ, Berkun Y, et al. JAK1/2 inhibition with baricitinib in the treatment of autoinflammatory interferonopathies. J Clin Invest. 2018 Jul 2;128(7):3041–52.

Figure Legends

Figure. 1 Clinical phenotype of proband with homozygous p.Y95C *DNASE2* variant. **(A)** Pedigree shows segregation of the p.Y95C homozygous DNASE-II variant. **(B)** MRI of V-2 showing bilateral deep white matter lesions (yellow arrows). **(C)** Haemophagocytosis and macrophage infiltration in bone marrow (x200 on right). **(D)** Multiple sequence alignment across different species of the p.Y95C mutation. **(E)** Predicted crystal structure of DNase II showing the mutations p.Y95C, p.G116A and p.D121V. **(F)** Densitometric quantification of the gel band intensity (left) and representative agarose gel of patient and control lysates incubated with 1Kbp ladder (right) **(G)** Serum cytokine quantification from V-2 (4 time points across 35 months), and healthy donors (n=24) tested by Meso Scale Discovery (MSD). Mann-Whitney U test,****p<0.0001.

Figure. 2 Clinical and immunological response to JAK1/JAK2 blockade with baricitinib treatment in patient V-2. (A) Height and weight of patient (normal range in grey, WHO normative data in black lines). **(B)** Haemoglobin (Hb), ferritin, platelets and calprotectin (normal range in grey). Blue arrows indicate start of baricitinib. **(C)** Quantitative qPCR of a

panel of interferon stimulated genes (ISGs) and **(D)** *IL-18* measured in whole blood of patient V-2 at 2 time points pre-treatment and 2 post-treatment, normalized to controls. **(E)** Serum cytokine MSD quantification from patient V-2 (collected 2 times pre-treatment and 1 post-treatment), normalized to controls.

A

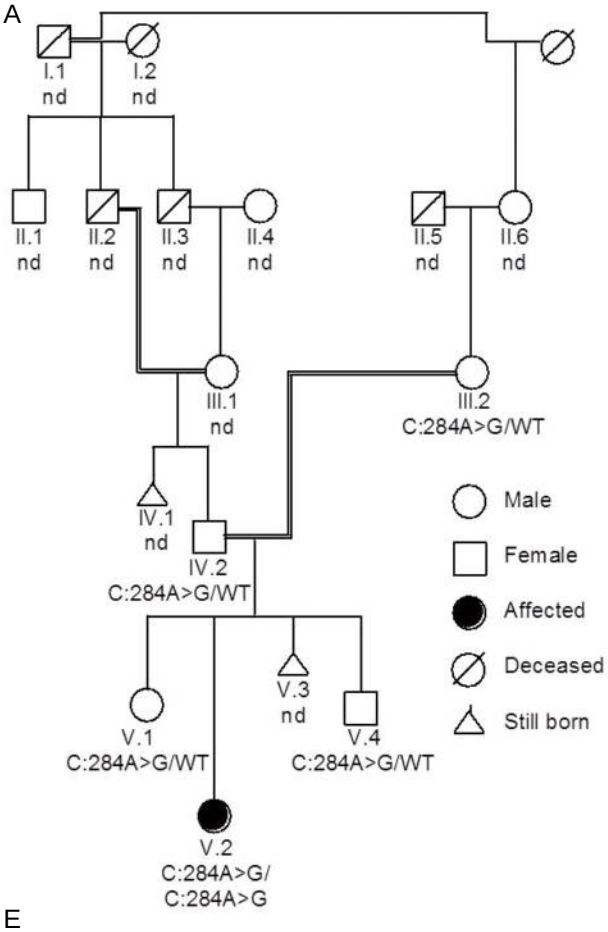

B

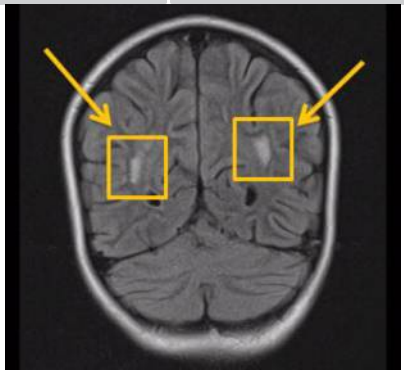

C

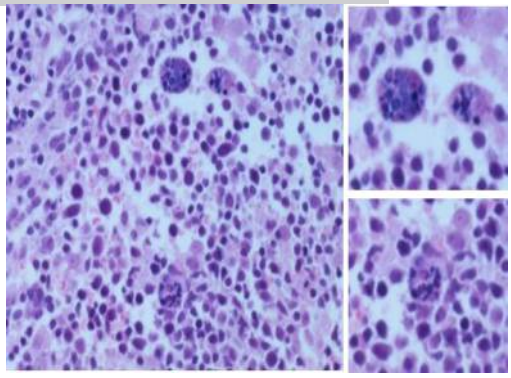

D

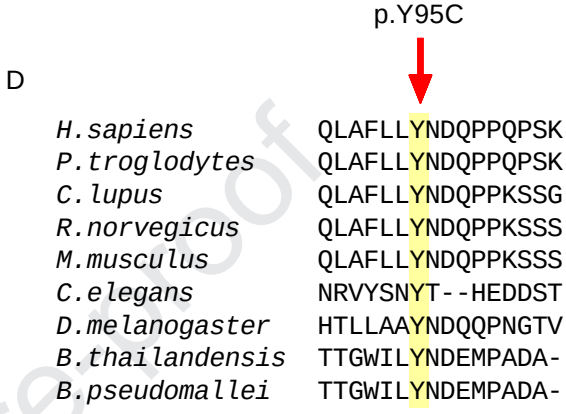

E

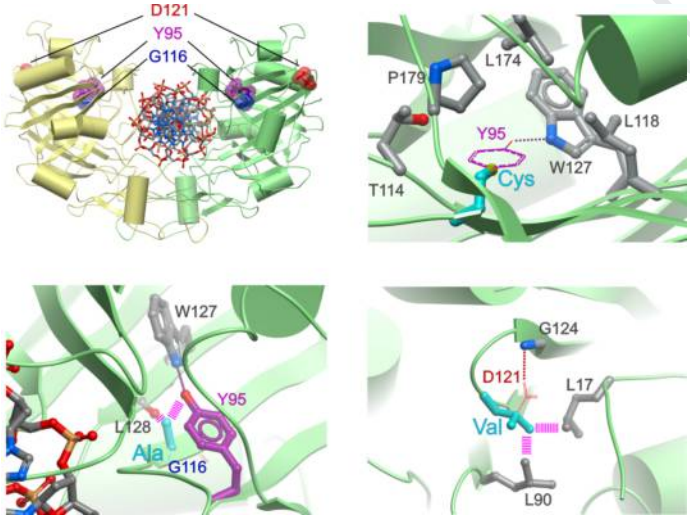

F

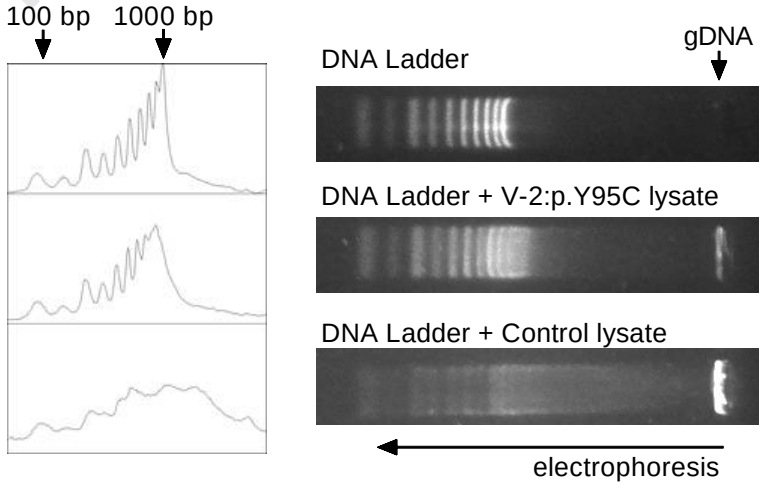

G

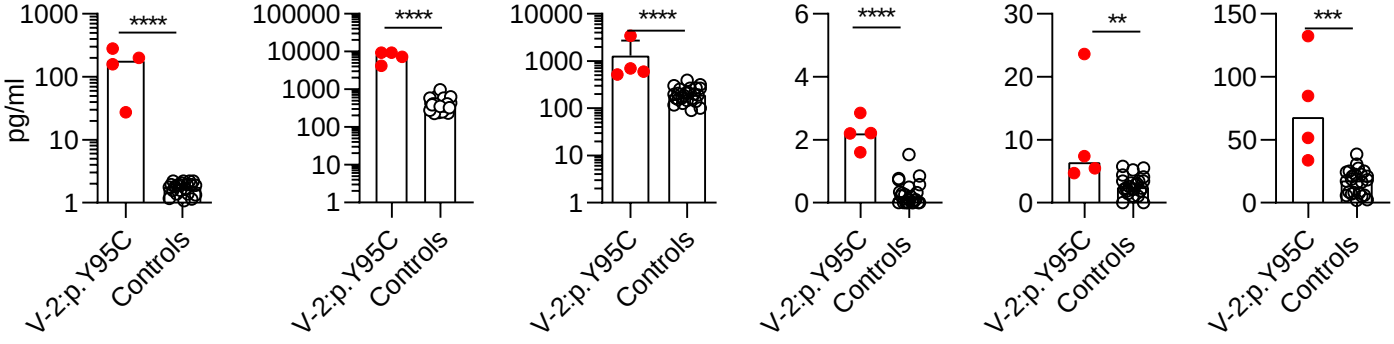

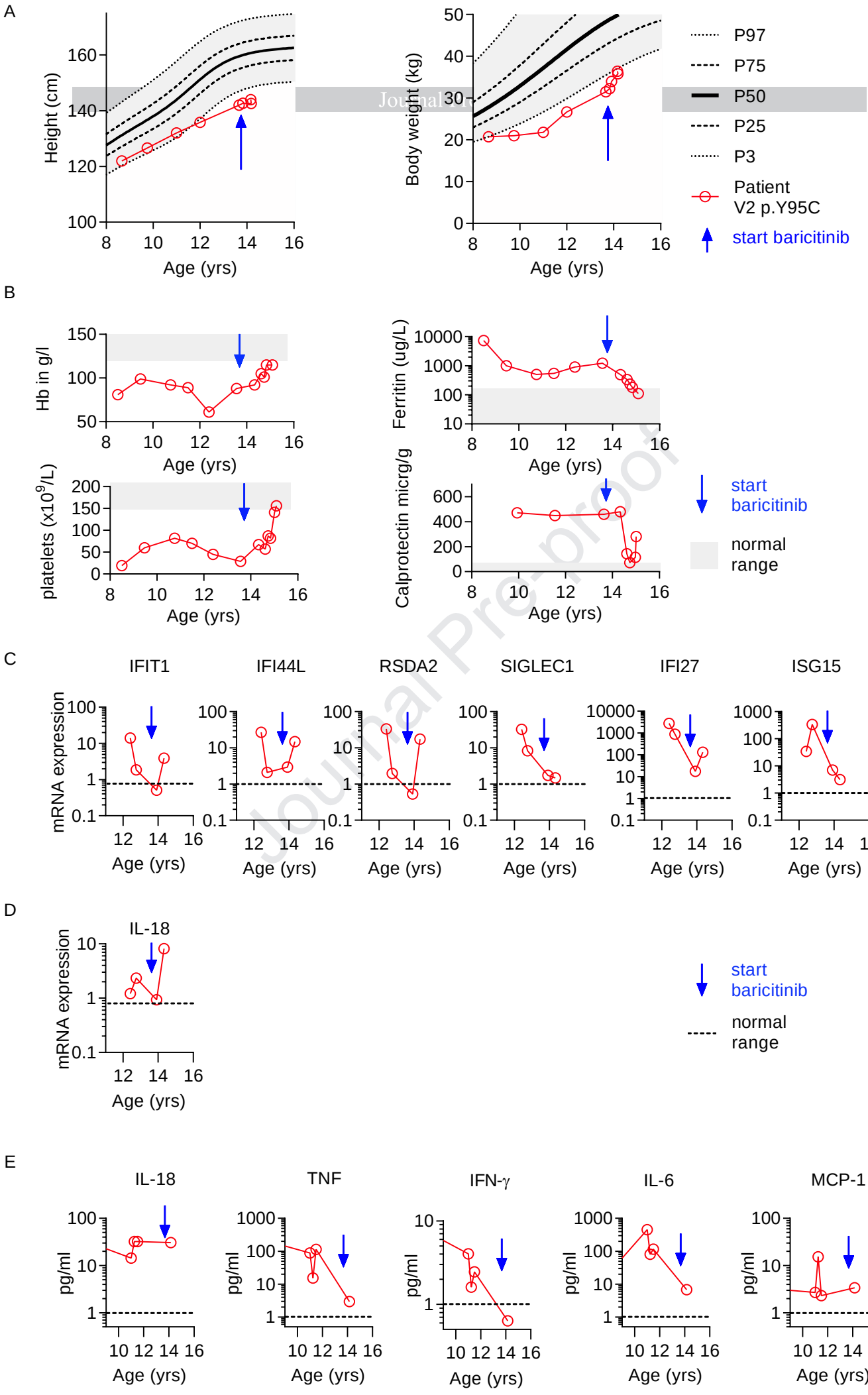
A
Height (cm)
Age (yrs)
Body weight (kg)
P97
P75
P50
P25
P3
Patient
V2 p.Y95C
start baricitinib
B
Hb in g/l
Ferritin (ug/L)
platelets (x10^9/L)
Calprotectin micrg/g
start
baricitinib
normal
range
C
IFIT1
IFI44L
RSDA2
SIGLEC1
IFI27
ISG15
mRNA expression
D
IL-18
E
IL-18
TNF
IFN-γ
IL-6
MCP-1
pg/ml

Material and Methods

Study participants

This study was approved by the Bloomsbury ethics committee (ethics number 08H071382), Oxford GI biobank (ethics number 09/H1204/30) and the Comité de Protection des Personnes (ID-RCB/EUDRACT: 2014-A01017-40) in France; we obtained written informed consent from all the family members and adolescent healthy controls with local ethics approval (REC 11/LO/0330).

Genetic mapping and sequencing

All five family members were genotyped using the Illumina cytoSNP12 chip. 200ng of DNA was isothermally amplified overnight and then enzymatically fragmented. The fragmented DNA was incubated on a BeadChip overnight. These were imaged using the Illumina iScan Read. The regions of homozygosity were identified using Illumina's Beadstudio with the Loss of Heterozygosity detector plug-in (version 1.0.3). The minimum number of contiguous homozygous SNPs was set to 100.

Whole exome sequencing was completed using the Illumina platform and sequenced on the Illumina HiSeq2000. The raw sequence data was aligned to the human reference genome using the Burrows-Wheeler Aligner (BWA) alignment algorithm. Variant calling was performed with the Genome Analysis Toolkit (GATK) and variants were annotated with wANNOVAR.

The *DNASE2* variant was confirmed and familial segregation ascertained by PCR and Sanger sequencing using the following primers to amplify and sequence exon 3 (forward GCCTTCTCTTCCCTCTCTCC and reverse GTCAGGGGTTACCTTGGAAAAAT). Sanger sequencing was performed using the AB3730 using the BigDye v3.1 kit (Applied Biosystems).

Protein sequence alignment

Multiple DNASE2 sequences were aligned using ClustalW2 (Goujon et al., 2010). Data were obtained from the Sequence alignment is based on the following National Center for Biotechnology Information (NCBI accession numbers). *Homo sapiens* AAH10419.3, *Rattus norvegicus* NP_612548.1, *Pan troglodytes* XP_001170388.1, *Canis lupus* XP_533902.3, *Mus musculus* NP_034192.1, *Drosophila melanogaster* NP_650672.1, *Caenorhabditis elegans*

NP_491414, *Burkholderia thailandensis* WP_009895252.1, *Burkholderia pseudomallei* YP_111989.1.

Structural modelling

Structural models and figures were prepared using the ICM software package (Molsoft). A homology model for human DNase II was prepared using the existing structure from *Burkholderia thailandensis* (PDB 5unb) as the model template. Double-stranded DNA (PDB 2bna) was positioned manually at the dimer interface to indicate the potential DNA binding surface as previously highlighted (10). All coordinate files were obtained from the Protein Data Bank (http://www.rcsb.org).

PBMC isolation and monocyte-derived macrophage cell culture

Peripheral blood mononuclear cells (PBMCs) were isolated from 15 ml of blood from patient and from controls by density gradient centrifugation (Lymphoprep; StemCell Technologies, Inc.) and cultured in RPMI1640 medium with glutamine (Sigma-Aldrich) supplemented with 10% FCS. 4 x 10^6 PBMC were plated and after 2 hours, adherent monocytes were washed and cultured in presence of 100 ng/ml of M-CSF (Peprotech) for 5 days in order to differentiate them to macrophages. PBMCs were FACS-sorted from healthy donor bloods using canonical cell population surface markers. Dendritic cells CD1c+ (clone B-Ly6, BD Biosciences), B cells CD19+ (Clone HIB19, BioLegend) and CD8+ (clone RPA-T8, Biosciences), T cells CD4+ (Clone RM4-5, BioLegend), T memory cells CD45RO (clone UCHL1, BioLegend) and CCR7 (clone G043H7, BioLegend), T cells CD8+ (clone RPA-T8, Biosciences), DR+11C- (Clone B-Ly6, BD Biosciences), NK cells CD16+ (clone 3G8, BioLegend), myeloid DCs CD141+ (clone M80, BioLegend) and monocytes CD14+ (clone M5E2, BioLegend).

DNA degradation assay in granulocytes and COS-7 cells

Granulocytes were purified from the precipitate after the blood gradient by removing red blood cells with ACK lysis buffer (Invitrogen). 3.5 x 10^6 granulocytes from patient and controls were lysed in 40 µl of lysis buffer (25 mM Tris-HCl pH 7.6, 150 mM NaCl, 5 mM EDTA, 1% NP-40 or 1% Triton X-100, 1% sodium deoxycholate, 0.1% SDS) at pH 5.5 in presence of proteinase and phosphates inhibitors. Lysates were spun down at 14000 rpm for 15 min and supernatants were collected. Each lysate was split in two; 20 µl incubated with 2 µl of 1Kbp DNA ladder solution (Bioline) and 20 µl without. Samples were incubated for 90 mins at 37^{O}C.

10 µl of each sample was loaded on agarose gel (1.5 %) and run under electric field at 110V in presence of TAE 1X buffer for 1hour. Gel pictures were acquired at UVP BioImaging System. Gel densitometry analysis was done by use of ImageJ program.

Human *DNASE2* cDNA sequence was cloned into the expression pcDNA3.1 (+) vector (Invitrogen, San Diego, CA) (11) and used as a wild-type construct. The variant construct corresponding to p.Y95C in *DNASE2* was inserted into the wild type template using the KOD-Plus Mutagenesis kit (Toyobo Co., Ltd., Osaka, Japan). Nucleotide sequences of the construct were confirmed by DNA sequence analysis. Purification of each construct used for transfection was performed using the Plasmid Midi kit (Qiagen).

DNase II activity in the transfected COS-7 cells was assayed by the single radial enzyme diffusion method using a LAS-3000 imaging analyzer (Fuji Film, Tokyo, Japan) according to our previous reports (12). The activity of wild-type DNase II was defined as 1.0, and that of the amino acid-substituted DNase II was expressed relative to the wild type.

Immunofluorescence cell staining

2 x 10^5 macrophages from controls and patient were seeded on cyto-chamber and left to adhere for 2 hours. Subsequently they were stained with DAPI (1µg/ml, Sigma Aldrich) for 20 minutes and washed twice with PBS. To evaluate the ability of macrophages to process DNA from engulfed apoptotic cells, they were co-cultured for 4 hours with Sybr-Green (1:10000, Life Technologies) positive HEK293 apoptotic cells in a ratio 1:1. Apoptosis was induced by exposition under UV lamp for 20 minutes following 4 hours of culture; the apoptosis status was confirmed by FACS staining for AnnexinV and 7AAD. Moreover to evaluate the ability of macrophages to process DNA from invasive *Salmonella*, they were infected for 1 hour with Syto-9 (50 nM, Life Technologies) positive bacteria at MOI 1:10 and then left for 4 hours under gentamicin treatment. In all the conditions 2 hours before the end of incubation, macrophages were stained with Lyso-tracker deep red (Thermo Fisher) 1:2000 solution. Cells were fixed with PBS-PFA 4% solution for 10 minutes at 37 C and then washed. Slides were mounted with a glass coverslip by using vectashield solution (Vector Laboratories). Images were captured using a Nikon eclipse ME600 fluorescence microscope, and analyzed with ImageJ.

Gentamycin protection assay

Macrophages at day 5 of differentiation were detached with Versene (Gibco) for 5 minutes and counted. 2 x10^4 macrophages were seeded per well in 96 well plates. Then, they were infected

with *Salmonella typhimurium* at MOI 1:10 for 1 hour. Followed 2 hours of treatment with 100 µg/ml of gentamicin (Sigma-Aldrich). Cells were then lysates in 50 µl of Triton 1X. Undiluted and diluted 1:10 and 1:100 cell lysates were plated in LB-agar plates that were incubated O.N. at 37^{o}C. Bacterial colonies were manually counted.

Macrophage and fibroblast stimulations

Healthy donor macrophages (1x10^5 cells) and fibroblasts (1x10^5 cells) were either left untreated or treated with baricitinib (300nM, Cayman Chemical), AG490 (20µM, Calbiochem) and filgotinib (200nM, Cayman Chemicals) for 1 hour in 48well plate. Following treatment, both macrophages and fibroblasts were either left unstimulated or stimulated with IFN-α (10units/ml, R&D Systems) for 24 hours in the presence of the drug.

RNA expression analysis in total blood, fibroblasts and macrophages.

Whole blood was collected into PAXgene tubes. We used a PreAnalytix RNA isolation kit for whole blood and the RNeasy Micro Kit (Qiagen) for RNA isolation from macrophages and fibroblasts. The RNA concentration was assessed with a Nanodrop (FLUOstar Omega, Labtech). Total RNA was retrotranscribed to cDNA using the Reverse Transcription kit (Applied Biosystems). We performed quantitative polymerase chain reaction (qPCR) analysis using the iTaq Universal SYBR Green Supermix (172-5121, Bio-Rad) and the TaqMan Gene Expression Assay (FAM) (Applied Biosystems).

The relative abundance of each of 6 ‘interferon score’ target (IFL27, IFIT1, IFI44L, ISG15 and RSAD2) and other pro inflammatory transcripts was normalized to the expression level of HPRT1 or RPLPO assessed using Bio Rad CFX Maestro software.

Cytokine protein analysis using ELISA and multiplex assay

Cytokine levels were measured in the serum of patients and controls, and in supernatants of fibroblasts using a Meso Scale Discovery (MSD) multiplex kit (Meso Scale Diagnostics), as per the manufacturer’s instructions in patients, and controls. Control sera was obtained from adolescent healthy controls with local ethics approval (REC reference 11/LO/0330; *n* = 24; 13 males; median age, 15.7 year; range, 10.7 – 17.5 year). Undiluted macrophage supernatants were assayed for TNF, IL1-ß and IL18 cytokines using ProcartaPlex-Multiplex Immunoassay (Invitrogen).

Statistical analyses

All statistics (ANOVA, or Mann Whitney U test) graphs were produced using Prism version 8 (GraphPad). All experiments were repeated in as a minimum in triplicate, unless otherwise specified. $P < 0.05$ was considered significant.

Supplementary Table 1: Patient V-2 laboratory investigations.

MHC, Major Histocompatibility Complex; HLH, haemophagocytic lymphohistiocytosis.

Laboratory investigations	Patient V-2 (Reference range)
Autoantibodies persistent >3 months	Absent[1]
*Haemoglobin	50g/L [2] (120-160)
*Platelet count	21x10^9/L [3] (150-450)
*White blood cell count	0.24 x10^9/L [4] (4.0-11)
*Triglycerides	3.98 mmol/L (0.32-1.46)
Fibrinogen	2.9 g/L (1.7-4.0)
Monocyte and lymphocyte subsets	Lymphopenia[5]
	Normal alpha beta double negative T cells
	Normal gamma delta T cells
Naïve T cell subsets	Variable[6]
Immunoglobulin G	19.9 g/L (3.1-13.8)
Immunoglobulin A	1.94 g/L (0.4-0.7)
Immunoglobulin M	2.29 g/L (0.5-2.2)
Immunoglobulin D	7 kU/L (2-100)
Immunoglobulin E	5.1 kU/l (0 – 48)
MHC Class I Expression	Normal
T Cell V Beta Repertoire	Consistent with polyclonal T cells
Interleukin-2-Inducible T-Cell Kinase ITK Immunoblot	Normal
Nitroblue tetrazolium test	Normal
Vaccine responses	Variable[7]
Perforin expression (CD56 cells)	Normal[8]
Perforin Gene Sequencing	No damaging mutations[9]

*Laboratory features contributing to the diagnosis of haemophagocytic lymphohistiocytosis (HLH). Other clinical features supporting the diagnosis of HLH included fever, hepato-splenomegaly, and haemophagocytosis demonstrated in bone marrow aspirate (see main text).

[1] Autoantibodies tested: antinuclear antibodies, anti-neutrophil cytoplasm antibodies, rheumatoid factor, anti-tissue transglutaminase antibodies, anti-thyroid peroxidase antibodies
[2] lowest Hb level of 147 measurements
[3] lowest platelet count of 147 measurements.
[4] lowest white blood cell count of 147 measurements.
[5] Normal proportions of T B and NK cells but in low numbers.

CD107a granule release (CD8 and NK cells)	CD8 CD107a^{+} Control 5.0% Patient 6.9% NK CD107a Control 13.7% Patient 23.1%
*Natural Killer Cytotoxicity Test	Abnormal [10]
Gene Sequencing for known causes of HLH and immunodeficiency[11]	No known disease causing mutations identified
T cell receptor excision circles	1902 (>10,000/million T Cells) [12]
*Soluble CD25	7624 pg/ml[13] (<2500)[14]
Complement C3	1.49 g/L (0.75-1.65)
Complement C4	0.45 g/L (0.14-0.54)
Faecal Calprotectin	472 mg/kg[15] (<50)
*Ferritin	7371 mcg/L[16] (12-81)
Liver enzymes	ALT 219 U/L (10 – 25) Alkaline phosphatase 96 U/L (150-380)
PHA stimulation	Variable[17]

[6] Test repeated four times; normal proportion of naïve cells on three occasions (54-64%), reduced naïve T cells for age on one occasion (35%).
[7] IgG antibodies to tetanus normal (0.04IU/ml range >0.1IU/ml), IgG antibodies to pneumococcus all <0.35µg/ml range >0.35 µg/ml
[8] Very few cells available for analysis. Perforin expressed but quantification was not possible.
[9] One synonymous polymorphism in *PRF1*, c.C900T p.H330H identified Exome Aggregation Consortium frequency 63%.
[10] Test only completed on one occasion, subsequent efforts hampered by insufficient cells
[11] TIGER – **T**argeted **I**mmuno and **G**astro **E**n**R**ichement panel, covering 72 genes implicated in immunodeficiency and 53 genes implicated in diseases of interest to gastroenterology.
[12] Low for age
[13] Highest of two repeats, range 4301-4702pg/ml
[14] Healthy children and adults have sCD25 levels less than 2500pg/ml. Children with inflammation have levels of 2500pg/ml or higher. To date, genetically confirmed HLHs typically have had sCD25 levels of over 5000pg/ml but this decreases with treatment.
[15] Highest value of two measurements range 450-472 mg/kg
[16] Highest value of 43 measurements 7371ng/ml.
[17] Test repeated 8 times, 2 times normal result, four times absent, 1 time impaired, 1 time unable to analyse.

Supplementary Table 2: List of 18 candidate genes identified following homozygosity mapping and whole exome sequencing (see main text). Predicted impact of variant on protein summarised from wANNOVAR annotation. SIFT/PolyPhen2 Predictions: D – Deleterious, M – Medium, T –Tolerated, P – Polymorphism. Frequency (< 0.01) in population taken from 1000 genome and the Exome Sequencing Project. Genes highlighted in bold were considered for further study following filtering based on population frequency, and biological plausibility (see main text).

Gene	Variant	Predicted impact on protein from wANNOVAR summary	Commentary
ANP32C	c.C592A: p.Q198K	Unknown	Excluded from further consideration
APC2	c.C796A:p.P266T	SIFT – T, Polyphen2 - P	Excluded from further consideration
VMAC	**c.C328T:p.R110C**	**SIFT – T, Polyphen 2 -B**	**Variant not confirmed following Sanger sequencing (i.e. false positive), so discounted**
EMR1	c.A2180T:p.E727V	PolyPhen 2- B, present in 1% population	Excluded from further consideration
KANK 3	c.G2078A:p.S693N	SIFT – T, Polyphen2 – D, present in 1% population	Excluded from further consideration
MUC16	**c.G22123C:p.A7375 P**	**SIFT – D, Polyphen2 - D**	**Confirmed on Sanger sequencing but ultimately deemed biologically implausible candidate.**
ZNF560	c.G1253A:p.G418D	SIFT – T, Polyphen2 B, present in 1% of population	Excluded from further consideration
LDLR	c.G910A:p.D304N	SIFT – T, Polyphen 2 - B	Biologically implausible candidate. Excluded from further consideration
DNASE2	**c.A284G:p.Y95C**	**SIFT – D, Polyphen2 -D**	**Confirmed on Sanger sequencing. Final variant selected for further in-depth functional work (see main text).**

OR10C1	c.A736T:p.M246L	SIFT – D, Polyphen2 - B	Excluded from further consideration
VARS2	**c.G2308A:p.V770M**	**SIFT – T, Polyphen2 - D**	**Confirmed on Sanger sequencing. This variant causes mitochondrial disease (wrong phenotype), and ultimately excluded in V-2 following normal respiratory chain enzyme analysis of muscle biopsy specimen.**
MUC22	c.C323G:p.T108S	No prediction	Excluded from further consideration
HLA-B	c.C341A:p.A114D c.A301G:p.S101G	SIFT – T, Polyphen2 – B SIFT – T, Polyphen2 - B	Biologically implausible candidate; excluded from further consideration
MICA	**c.G493A:p.V165I**	**SIFT – T, Polyphen2 - B**	**Confirmed on Sanger sequencing; highly polymorphic gene, predicted non-damaging variant, so excluded**
LY6G6F	**c.G442C:p.V148L**	**SIFT – D, Polyphen2 - D**	**Confirmed on Sanger sequencing; involved in platelet activation therefore biologically less plausible candidate**
HLA-DRB5	c.C308T:p.A103V c.G307C:p.A103P	SIFT – T, Polyphen2 – P SIFT – T, Polyphen2 - P	Excluded from further consideration
HLA-DQA1	c.C592A:p.Q198K	SIFT – T, Polyphen2 - B	Excluded from further consideration

Figure.S1 Homozygous mutation that leads to loss of function of *DNaseII*, but not to mRNA or protein level changes in cells. (A) Sanger sequencing chromatogram of *DNASE2* aligned to reference exon 3 (NM_001375) at position c.284. showing a heterozygous pattern with parents (IV-2, III-2) and unaffected siblings (V-1 and V-4) of the proband, and homozygosity for G in the affected proband (V-2). **(B)** A single radial enzyme diffusion assay revealed that substitution of the tyrosine at amino acid 95 with a cysteine (p.Y95C) completely abolishes DNase II activity in COS-7 cells. There was no change of *DNASE2* protein expression **(C)** or mRNA **(D)** in V-2 dermal fibroblasts

Figure. S2 Macrophages with the homozygous *DNASE2* p.Y95C variant have impaired DNA clearance ability. (A) *DNASE2* gene expression of sorted human cells from heathy controls reveals that macrophages show highest expression of *DNASE2*. ***p<0.0001. **(B)** Confocal image (left) and quantification of DNA in lysosomes (right) of patient and control macrophages stained with DAPI and Lysotracker. There was increased lysosomal DNA accumulation in monocyte-derived macrophages from V-2 compared to controls. **(C)** Confocal image (left) and quantification of exogenous DNA in lysosome per cell (right) of patient and control macrophages stained with DAPI and then co-cultured with Sybr-Green positive apoptotic HEK293 cells and **(D)** pre-stained Syto9-*Salmonella* (MOI:20); Monocyte derived macrophages from patient V-2 and two previously reported siblings with homozygous p.G116A mutation showed reduced clearance of exogenous apoptotic or bacterial derived DNA. **(E)** Gentamicin protection assay of monocyte-derived macrophages from patient V-2 and controls showed normal antimicrobial activity. Graph represents pooled data of colony forming unit (CFU) quantification.

Figure S3 Pro-inflammatory cytokine profile in fibroblasts and macrophages derived from proband V-2 with homozygous p.Y95C *DNASE2* variant (A) Increased levels of cytokine (TNF, IL-1β, IP-10 and IL-8) quantified by ELISA and upregulation of gene expression of the ISGs genes (*IFIT1* and *IFI44L*) in V-2 fibroblasts compared to control cells. **(B)** Increased levels of cytokine (TNF, IL-18 and IL1β) quantified by Luminex and upregulation of gene expression of the ISGs genes (IFIT1 and IFI44L) in V-2 macrophages compared to control cells. Gene expression of the interferon stimulated genes (*IFIT1* and *IFI44L*) in macrophages from a patient with homozygous *DNASE2* p.G116A variant and healthy control macrophages was also performed, and is presented for comparison.

Figure S.4. Impact of *in vitro* JAK1/JAK2 blockade on type I interferon signature and IL18 expression. (A) Quantitative RT-PCR of interferon stimulated genes (ISGs: *IFIT1, IFI44L, RSDA2, SIGLEC1, IFI27*) from patient V-2 and control fibroblasts with and without IFN-α stimulation, in the presence and absence of baricitinib (JAK1/JAK2 blockade), AG490 (selective JAK2 blockade) and filgotinib (selective JAK1 blockade) for 24 hours. **(B)** qPCR of ISGs (*IFIT1, IFI44L, RSDA2, SIGLEC1, IFI27*) from healthy donor macrophages stimulated with and without IFN-α, in the presence and absence of baricitinib or AG490 for 24 hours. **(C)** qPCR of *IL18* and *IL1β* genes from healthy donor macrophages stimulated with and without IFN-α, in the presence and absence of baricitinib and AG490 for 24 hours.

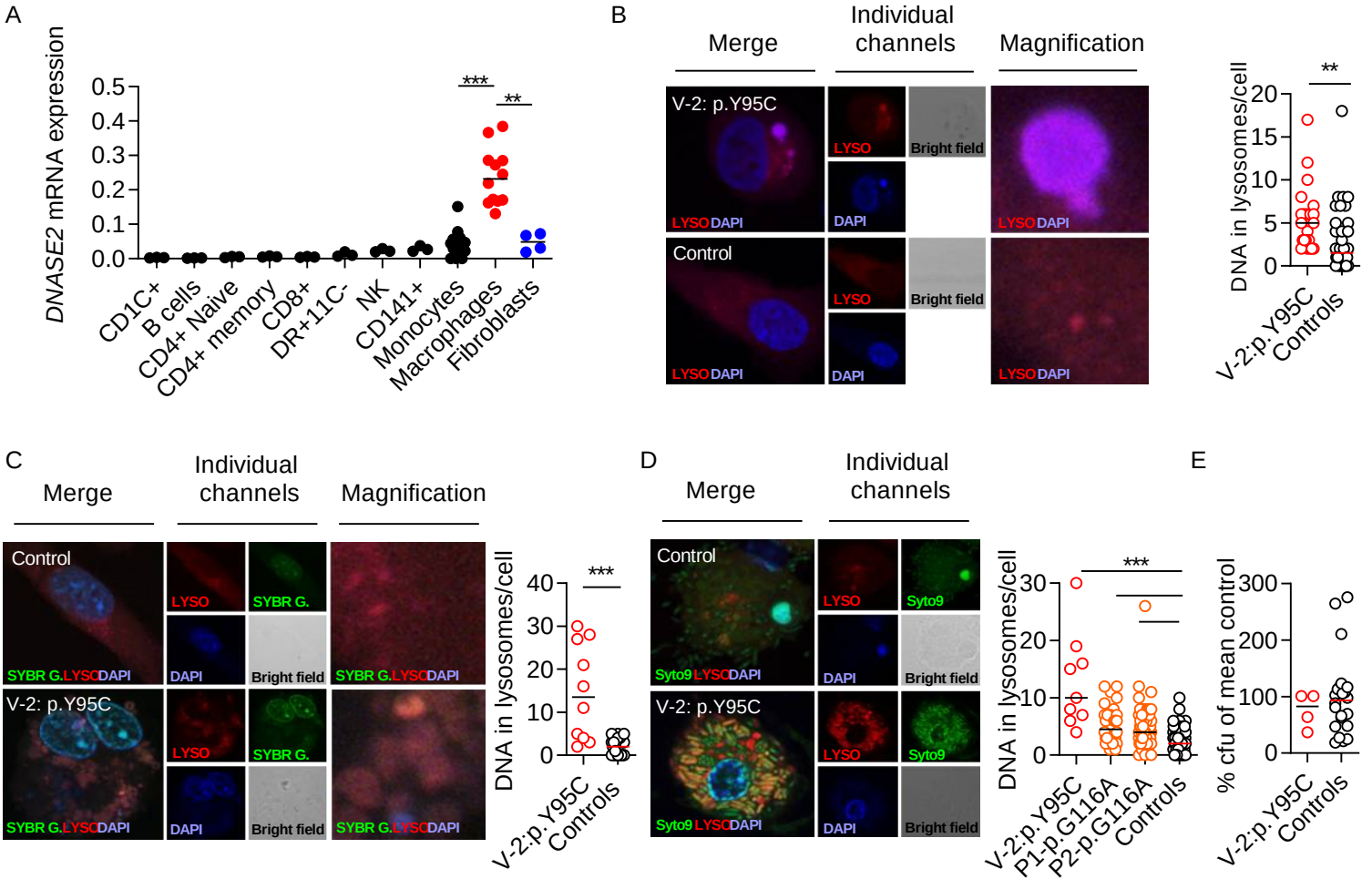
A
DNASE2 mRNA expression
0.5
0.4
0.3
0.2
0.1
0.0
***
**
CD1C+
B cells
CD4+ Naive
CD4+ memory
CD8+
DR+11C-
NK
CD141+
Monocytes
Macrophages
Fibroblasts
B
Merge
Individual channels
Magnification
V-2: p.Y95C
Control
LYSO
DAPI
Bright field
LYSO DAPI
DNA in lysosomes/cell
20
15
10
5
0
**
V-2:p.Y95C
Controls
C
Merge
Individual channels
Magnification
Control
V-2: p.Y95C
LYSO
SYBR G.
DAPI
Bright field
SYBR G.LYSODAPI
DNA in lysosomes/cell
40
30
20
10
0
***
V-2:p.Y95C
Controls
D
Merge
Individual channels
Control
V-2: p.Y95C
LYSO
Syto9
DAPI
Bright field
Syto9 LYSO DAPI
DNA in lysosomes/cell
30
20
10
0
***
V-2:p.Y95C
P1-p.G116A
P2-p.G116A
Controls
E
% cfu of mean control
300
200
100
0
V-2:p.Y95C
Controls

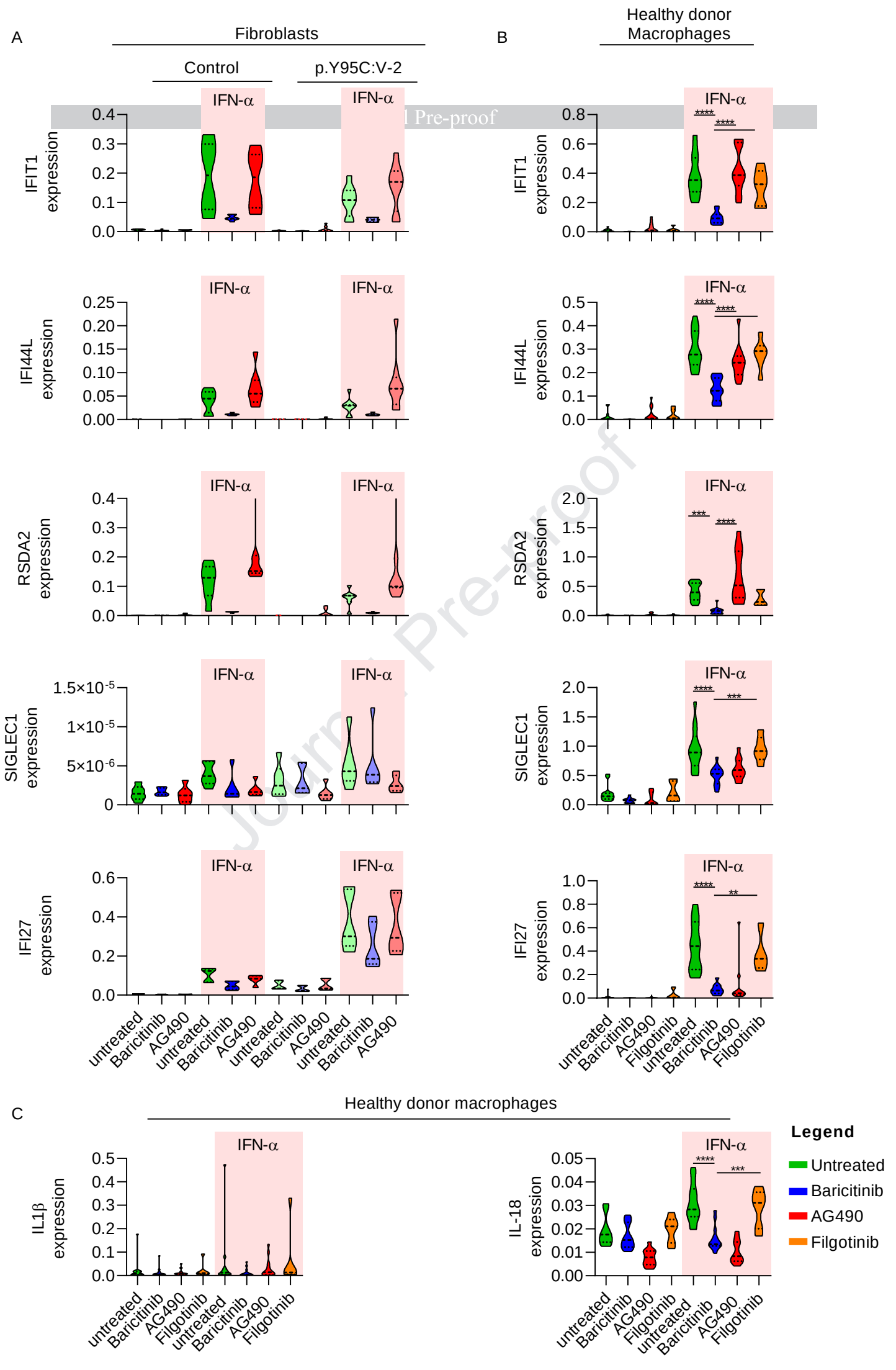

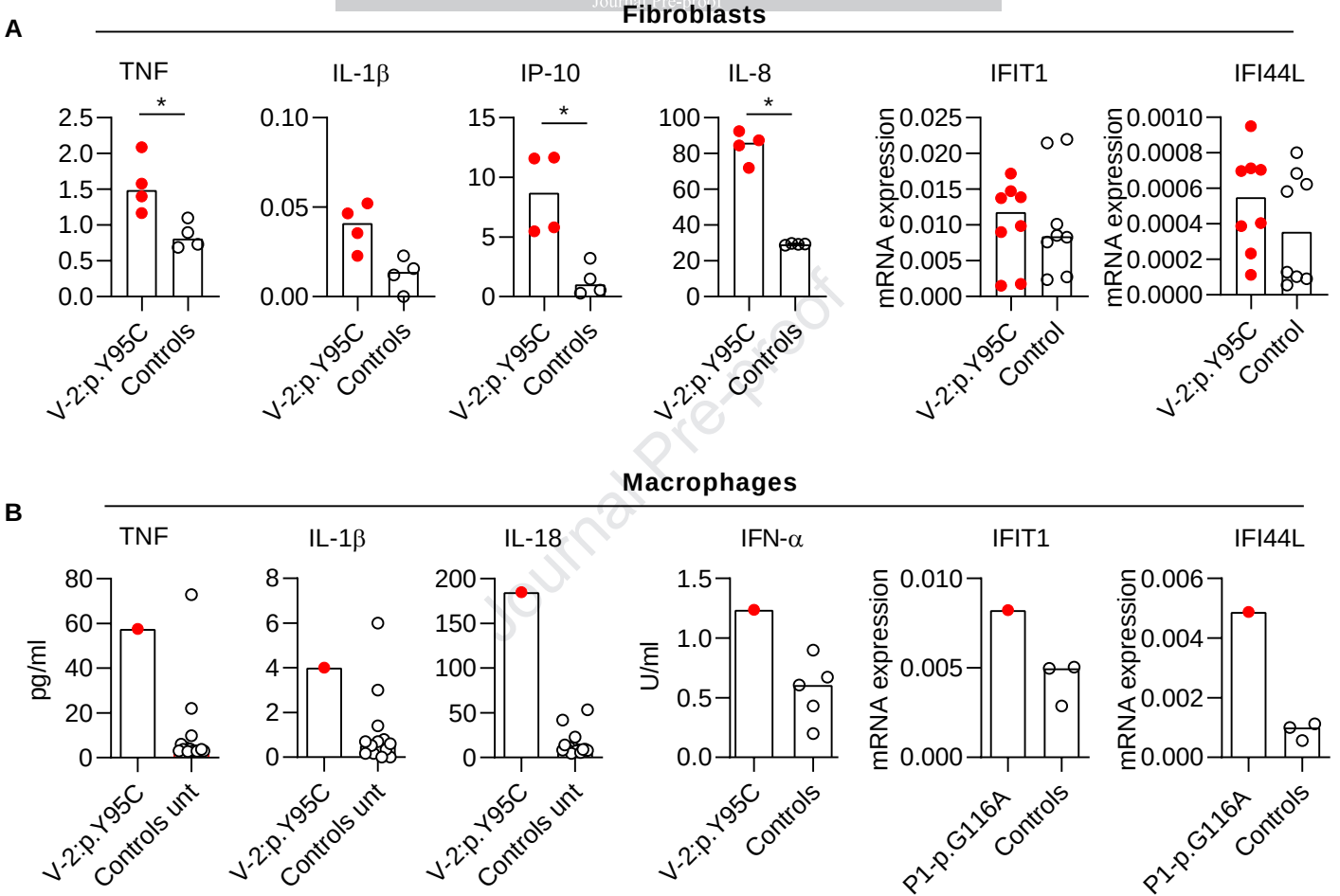

Sup.Fig.

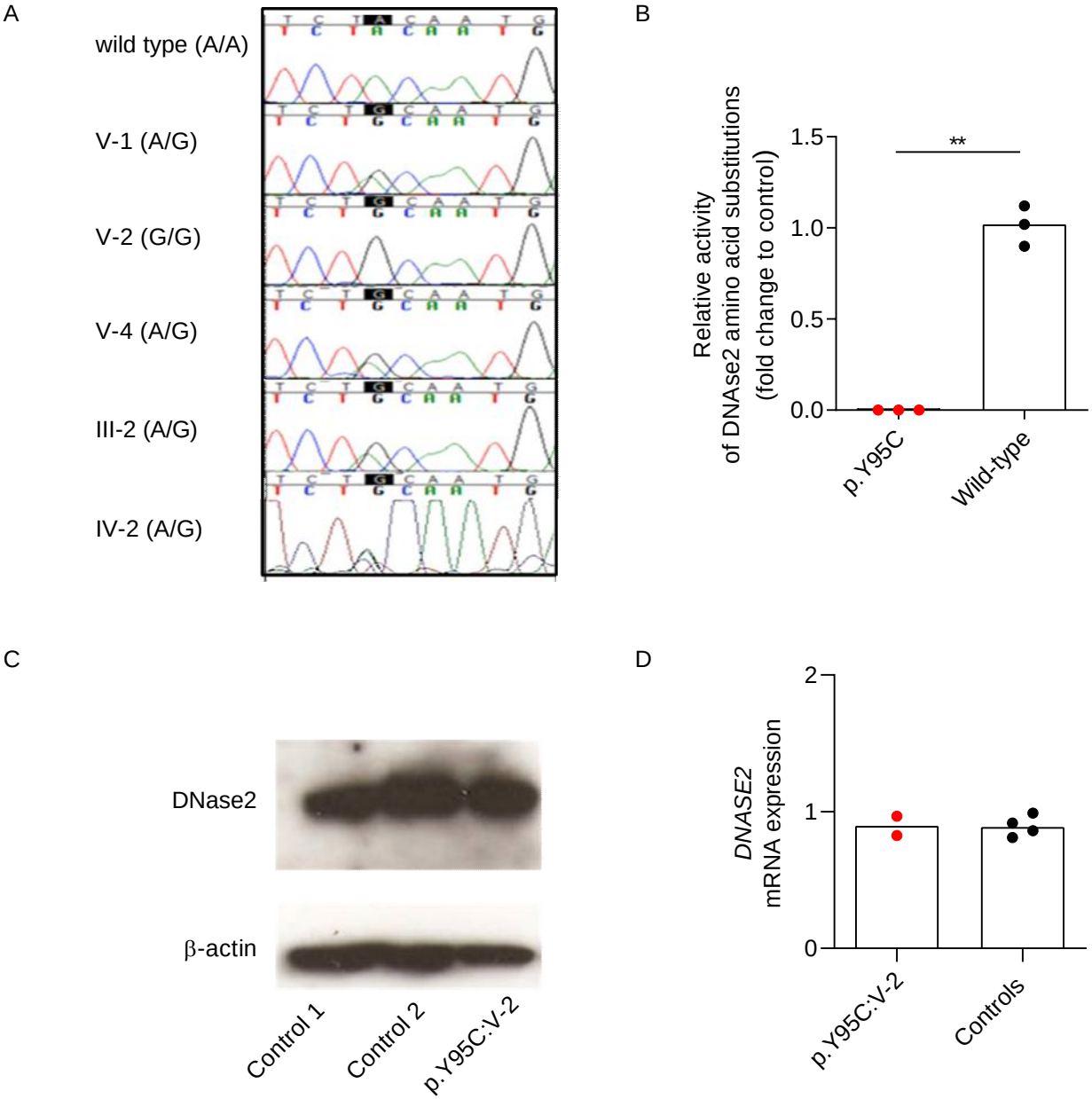
A
wild type (A/A)
V-1 (A/G)
V-2 (G/G)
V-4 (A/G)
III-2 (A/G)
IV-2 (A/G)
B
Relative activity
of DNAse2 amino acid substitutions
(fold change to control)
1.5
1.0
0.5
0.0
**
p.Y95C
Wild-type
C
DNase2
β-actin
Control 1
Control 2
p.Y95C:V-2
D
DNASE2
mRNA expression
2
1
0
p.Y95C:V-2
Controls